Comparative intrinsic optical signal imaging of wild-type and mutant mouse retinas

Qiu-Xiang Zhang,[1] Youwen Zhang,[2] Rong-Wen Lu,[1] Yi-Chao Li,[1] Steven J. Pittler,[2] Timothy W. Kraft,[2] and Xin-Cheng Yao[1,2,*]

[1]*Department of Biomedical Engineering, University of Alabama at Birmingham, Birmingham, AL 35294, USA*
[2] *Department of Vision Sciences, University of Alabama at Birmingham, Birmingham, AL 35294, USA*
[*]*xcy@uab.edu*

Abstract: Functional measurement is important for retinal study and disease diagnosis. Transient intrinsic optical signal (IOS) response, tightly correlated with functional stimulation, has been previously detected in normal retinas. In this paper, comparative IOS imaging of wild-type (WT) and rod-degenerated mutant mouse retinas is reported. Both 2-month and 1-year-old mice were measured. In 2-month-old mutant mice, time course and peak value of the stimulus-evoked IOS were significantly delayed (relative to stimulus onset) and reduced, respectively, compared to age matched WT mice. In 1-year-old mutant mice, stimulus-evoked IOS was totally absent. However, enhanced spontaneous IOS responses, which might reflect inner neural remodeling in diseased retina, were observed in both 2-month and 1-year-old mutant retinas. Our experiments demonstrate the potential of using IOS imaging for noninvasive and high resolution identification of disease-associated retinal dysfunctions. Moreover, high spatiotemporal resolution IOS imaging may also lead to advanced understanding of disease-associated neural remodeling in the retina.

OCIS codes: (170.2655) Functional monitoring and imaging; (170.4580) Optical diagnostics for medicine; (170.3880) Medical and biological imaging; (330.5380) Physiology.

References and links

1. C. A. Curcio, N. E. Medeiros, and C. L. Millican, "Photoreceptor loss in age-related macular degeneration," Invest. Ophthalmol. Vis. Sci. **37**(7), 1236–1249 (1996).
2. D. Nagy, B. Schönfisch, E. Zrenner, and H. Jägle, "Long-term follow-up of retinitis pigmentosa patients with multifocal electroretinography," Invest. Ophthalmol. Vis. Sci. **49**(10), 4664–4671 (2008).
3. Y. W. Qin, G. Z. Xu, and W. J. Wang, "Dendritic abnormalities in retinal ganglion cells of three-month diabetic rats," Curr. Eye Res. **31**(11), 967–974 (2006).
4. H. P. Scholl and E. Zrenner, "Electrophysiology in the investigation of acquired retinal disorders," Surv. Ophthalmol. **45**(1), 29–47 (2000).
5. D. C. Hood, "Assessing retinal function with the multifocal technique," Prog. Retin. Eye Res. **19**(5), 607–646 (2000).
6. K. Holthoff and O. W. Witte, "Intrinsic optical signals in vitro: a tool to measure alterations in extracellular space with two-dimensional resolution," Brain Res. Bull. **47**(6), 649–655 (1998).
7. R. D. Andrew, C. R. Jarvis, and A. S. Obeidat, "Potential sources of intrinsic optical signals imaged in live brain slices," Methods **18**(2), 185–196, 179 (1999).
8. M. Haller, S. L. Mironov, and D. W. Richter, "Intrinsic optical signals in respiratory brain stem regions of mice: neurotransmitters, neuromodulators, and metabolic stress," J. Neurophysiol. **86**(1), 412–421 (2001).
9. Y. C. Li, W. X. Cui, X. J. Wang, F. Amthor, R. W. Lu, A. Thompson, and X. C. Yao, "Intrinsic optical signal imaging of glucose-stimulated insulin secreting β-cells," Opt. Express **19**(1), 99–106 (2011).
10. X. C. Yao, A. Yamauchi, B. Perry, and J. S. George, "Rapid optical coherence tomography and recording functional scattering changes from activated frog retina," Appl. Opt. **44**(11), 2019–2023 (2005).
11. X. C. Yao and J. S. George, "Dynamic neuroimaging of retinal light responses using fast intrinsic optical signals," Neuroimage **33**(3), 898–906 (2006).
12. X. C. Yao and J. S. George, "Near-infrared imaging of fast intrinsic optical responses in visible light-activated amphibian retina," J. Biomed. Opt. **11**(6), 064030 (2006).

#159911 - $15.00 USD Received 12 Dec 2011; revised 19 Jan 2012; accepted 4 Feb 2012; published 20 Mar 2012

13. X. C. Yao and Y. B. Zhao, "Optical dissection of stimulus-evoked retinal activation," Opt. Express **16**(17), 12446–12459 (2008).
14. X. C. Yao, L. Liu, and Y. G. Li, "Intrinsic optical signal imaging of retinal activity in frog eye," J Innov Opt Health Sci **2**(02), 201–208 (2009).
15. Q. X. Zhang, J. Y. Wang, L. Liu, and X. C. Yao, "Microlens array recording of localized retinal responses," Opt. Lett. **35**(22), 3838–3840 (2010).
16. J. Schallek, H. Li, R. Kardon, Y. Kwon, M. Abramoff, P. Soliz, and D. Ts'o, "Stimulus-evoked intrinsic optical signals in the retina: spatial and temporal characteristics," Invest. Ophthalmol. Vis. Sci. **50**(10), 4865–4872 (2009).
17. Q.-X. Zhang, R.-W. Lu, Y.-G. Li, and X.-C. Yao, "In vivo confocal imaging of fast intrinsic optical signals correlated with frog retinal activation," Opt. Lett. **36**(23), 4692–4694 (2011).
18. V. J. Srinivasan, Y. Chen, J. S. Duker, and J. G. Fujimoto, "In vivo functional imaging of intrinsic scattering changes in the human retina with high-speed ultrahigh resolution OCT," Opt. Express **17**(5), 3861–3877 (2009).
19. R. S. Jonnal, J. Rha, Y. Zhang, B. Cense, W. H. Gao, and D. T. Miller, "In vivo functional imaging of human cone photoreceptors," Opt. Express **15**(24), 16141–16160 (2007).
20. T. Theelen, C. B. Hoyng, B. J. Klevering, and C. B, "Functional imaging of inherited retinal disease with a commercial optical coherence tomography," Proc. SPIE **8091**, 8009110–8009118 (2011).
21. Y. Zhang, L. L. Molday, R. S. Molday, S. S. Sarfare, M. L. Woodruff, G. L. Fain, T. W. Kraft, and S. J. Pittler, "Knockout of GARPs and the β-subunit of the rod cGMP-gated channel disrupts disk morphogenesis and rod outer segment structural integrity," J. Cell Sci. **122**(8), 1192–1200 (2009).
22. Y. G. Li, Q. X. Zhang, L. Liu, F. R. Amthor, and X. C. Yao, "High spatiotemporal resolution imaging of fast intrinsic optical signals activated by retinal flicker stimulation," Opt. Express **18**(7), 7210–7218 (2010).
23. G. L. Kesteven, "The coefficient of variation," Nature **158**(4015), 520–521 (1946).
24. X. Huang, W. Kong, Y. Zhou, and G. Gregori, "Distortion of axonal cytoskeleton: an early sign of glaucomatous damage," Invest. Ophthalmol. Vis. Sci. **52**(6), 2879–2888 (2011).
25. C. Gargini, E. Terzibasi, F. Mazzoni, and E. Strettoi, "Retinal organization in the retinal degeneration 10 (rd10) mutant mouse: a morphological and ERG study," J. Comp. Neurol. **500**(2), 222–238 (2007).
26. K. P. Hofmann, R. Uhl, W. Hoffmann, and W. Kreutz, "Measurements on fast light-induced light-scattering and -absorption changes in outer segments of vertebrate light sensitive rod cells," Biophys. Struct. Mech. **2**(1), 61–77 (1976).
27. H. Kühn, N. Bennett, M. Michel-Villaz, and M. Chabre, "Interactions between photoexcited rhodopsin and GTP-binding protein: kinetic and stoichiometric analyses from light-scattering changes," Proc. Natl. Acad. Sci. U.S.A. **78**(11), 6873–6877 (1981).
28. V. Y. Arshavsky, T. D. Lamb, and E. N. Pugh, Jr., "G proteins and phototransduction," Annu. Rev. Physiol. **64**(1), 153–187 (2002).
29. X. C. Yao, D. M. Rector, and J. S. George, "Optical lever recording of displacements from activated lobster nerve bundles and Nitella internodes," Appl. Opt. **42**(16), 2972–2978 (2003).
30. I. Tasaki and P. M. Byrne, "Rapid structural changes in nerve fibers evoked by electric current pulses," Biochem. Biophys. Res. Commun. **188**(2), 559–564 (1992).
31. G. H. Kim, P. Kosterin, A. L. Obaid, and B. M. Salzberg, "A mechanical spike accompanies the action potential in Mammalian nerve terminals," Biophys. J. **92**(9), 3122–3129 (2007).
32. L. B. Cohen, "Changes in neuron structure during action potential propagation and synaptic transmission," Physiol. Rev. **53**(2), 373–418 (1973).
33. R. E. Marc, B. W. Jones, C. B. Watt, and E. Strettoi, "Neural remodeling in retinal degeneration," Prog. Retin. Eye Res. **22**(5), 607–655 (2003).
34. S. F. Stasheff, "Emergence of sustained spontaneous hyperactivity and temporary preservation of OFF responses in ganglion cells of the retinal degeneration (rd1) mouse," J. Neurophysiol. **99**(3), 1408–1421 (2008).
35. J. Borowska, S. Trenholm, and G. B. Awatramani, "An intrinsic neural oscillator in the degenerating mouse retina," J. Neurosci. **31**(13), 5000–5012 (2011).

1. Introduction

Functional measurement is important for retinal study and diagnosis. Many eye diseases, such as age-related macular degeneration (AMD) [1], retinitis pigmentosa (RP) [2], diabetic retinopathy (DR) [3], and others, produce functional defects in the outer and/or inner retina. Morphological mapping of disease-associated structural abnormalities in the retina can provide valuable information for disease detection. In coordination with adaptive optics (AO) and optical coherence tomography (OCT), cellular resolution of retinal fundus imaging has been achieved. However, disease-associated morphological and functional changes are not always correlated directly, in terms of time course and spatial location. Therefore, objective assessment of retinal function is essential. Electrophysiological measurements, such as full field electroretinogram (ERG) [4] and relative multifocal ERG [5] are well established for objective evaluation of neural retinal dysfunction. However, signal specificities and resolution

#159911 - $15.00 USD Received 12 Dec 2011; revised 19 Jan 2012; accepted 4 Feb 2012; published 20 Mar 2012

of these ERG measurements are relatively low because of the integral effect of the electrophysiological changes over the whole depth of the retina.

Transient changes of intrinsic light properties (e.g., scattering, absorption, and polarization) in activated excitable cells can be used for functional imaging of living systems. Stimulus-evoked intrinsic optical signal (IOS) has been detected in nerve tissues [6–8], endocrine cells [9], and in the retina. IOS imaging may provide a noninvasive and high resolution method to evaluate functional integrity of the retina. Stimulus-evoked IOSs have been detected in isolated retinal tissues [10–15], intact animals [16, 17], and human subjects [18, 19]. Recently, IOS alterations were explored *in vivo* by OCT imaging of photoreceptors of patients with inherited retinal diseases [20]. The purpose of this study is to quantitatively compare temporal and spatial characteristics of IOS changes in normal and mutant retinas, and therefore to demonstrate the feasibility of using IOS imaging for high resolution identification of disease-associated retinal dysfunction.

A *Cngb1* knockout mouse model (Mus musculus) that does not express the β-subunit of the cGMP-gated cation channel and the related GARP proteins was employed for this study [21]. Rod function is attenuated but detectable up to 6 months. By 1 year of age the ERG response is no longer detectable and all rod cells have degenerated. In this paper, time courses and peak value of the IOS in normal and *Cngb1* retinas are quantitatively compared. Our experiments indicated that IOS onset-time and time-to-peak (relative to stimulus onset) of mutant mice were significantly delayed compared to wild-type (WT) mice. In addition, dynamic IOS background images, i.e., without retinal stimulation, revealed spontaneous activity-associated spatiotemporal patterns in the knockout mouse retina, while the WT mice had a relatively clean background.

2. Method

2.1 System setup

Figure 1 illustrates the schematic diagram of the experimental setup. Details of the optical imaging system have been reported in previous publications [14, 22]. Equipped with a high-speed CMOS camera (PCO1200, PCO AG, Kelheim, Germany), the imaging system provided millisecond temporal resolution and sub-cellular spatial resolution for dynamic monitoring of stimulus-evoked fast IOSs. As shown in Fig. 1, the imaging system consisted of two light sources: a near infrared (NIR) light for IOS recording, and a visible white light for retinal stimulation. The visible light produced by a fiber-coupled white light emitting diode (LED) was collimated to improve stimulation uniformity. A slit was placed behind the collimator to provide a rectangular stimulus of 80 μm x 180 μm. The NIR light produced by a 12-V 100-W halogen lamp (PHILIPS7724) was filtered by a band-pass filter (wavelength band: 800-1000 nm). The NIR filter, in front of the CMOS camera, was a long-pass filter which blocked visible stimulus light and transmitted NIR light that was detected. During the IOS recording, the retina was continuously illuminated by ~1 mW NIR light illumination. In each trial, pre-stimulus recording was 0.4 s, followed by a 10 ms visible light flash and 1.0 s post-stimulus recording. The raw images were captured at the frame rate of 1000 frames per second with image size of 400 x 300 pixels (240 μm x 180 μm).

2.2 Mice strains, handling, and genotyping

Knockout mice (Mus musculus) were generated as previously described [21] and maintained by homozygous crosses. Knockout mice originated in a 129 Sv background crossed into a C57Bl/6 background and were bred congenic (> 10 generations) prior to initiation of this study. Genotypes were verified as previously described [21] using standard PCR technology.

#159911 - $15.00 USD Received 12 Dec 2011; revised 19 Jan 2012; accepted 4 Feb 2012; published 20 Mar 2012

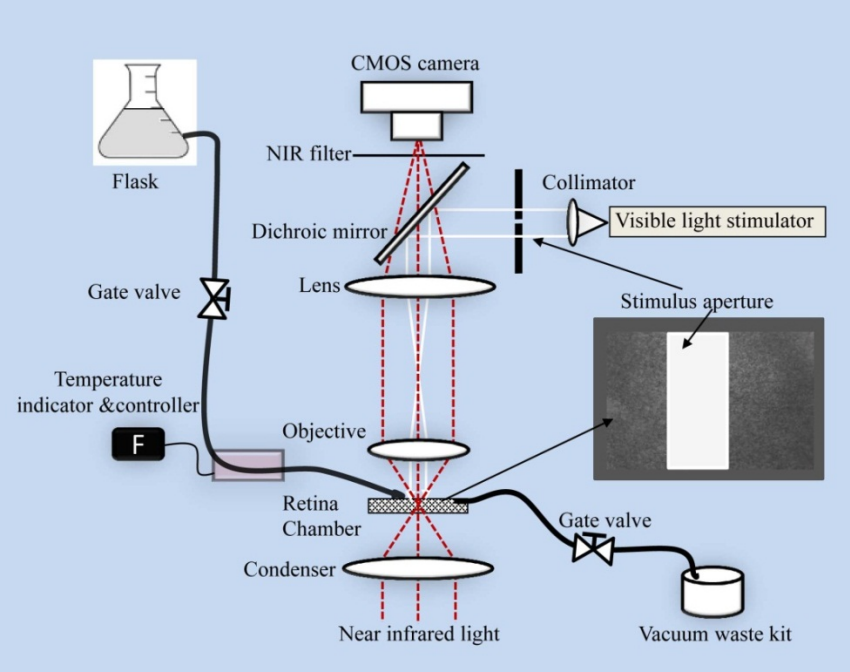

Fig. 1. Schematic diagram of experiment setup. A custom modified microscope, with 20x objective and high speed CMOS camera (10 bits depth and 1000 frames/s), was used for this study. During the measurement, the mouse retina was continuously illuminated by the NIR light for IOS recording; a 10 ms visible light flash was used for retinal stimulation.

WT mice were originally obtained from crosses of heterozygous knockout mice and maintained on a C57Bl/6 background. WT mice were verified by PCR [21] to be absent for the knockout allele. Mice were handled in accordance with university animal resources program guidelines and according to the ARVO "Statement for the Use of Animals in Ophthalmic and Visual Research". Mice were maintained on standard chow and water ad libitum and on a 12 on /12 off light cycle with overall light exposure limited to less than 300 lux.

2.3 Sample preparation

Isolated WT and *Cngb1* knockout mutant mouse retinas [21] (without retinal pigment epithelium) were used to test stimulus-evoked IOS responses. Without the complications of hemodynamic changes and eye movements, isolated retina is a simple preparation to verify the differences produced by retinal neuronal cells. The experiments were performed following the protocols approved by the Institutional Animal Care and Use Committee of University of Alabama at Birmingham. Briefly, retinal dissection was conducted in a dark room with dim red illumination. After overnight dark adaptation, eyeballs from anesthetized mice were rapidly enucleated and the retina was carefully isolated from the eyeball in Ames media, and then transferred to a recording chamber under a nylon grid mesh for IOS imaging. During the experiment, the sample was continuously super-fused (~2 ml/min) with oxygenated bicarbonate-buffered Ames medium, maintained at pH 7.4 and 33~37°C.

2.4 Data processing

IOS images shown in Figs. 2(b-d) are presented in the unit of $\Delta I/I$, where $\Delta I/$ is transient optical change and I is reference baseline. Dynamic differential data processing was employed to construct the IOS images [22]:

#159911 - $15.00 USD Received 12 Dec 2011; revised 19 Jan 2012; accepted 4 Feb 2012; published 20 Mar 2012

$$IOS_{t_i}(x,y)=\frac{\Delta I}{I}=\frac{I_{t_i}(x,y)-\frac{1}{m}\sum_{j=1}^{j=m}I_{t_{i-j}}(x,y)}{\frac{1}{m}\sum_{j=1}^{j=m}I_{t_{i-j}}(x,y)} \quad (1)$$

where $I_{t_i}(x,y)$ was the intensity at the time point of t_i, and i = 1,2,3, … represented the image index. m was the number of images before the image i. In other words, the dynamic reference baseline of the pixel at (x, y) was calculated by using the averaged pixel value of m consecutive frames recorded before the time point t_i. In this article, we selected m = 100 (i.e., images recorded over 100 ms).

Since the recording light intensities could increase or decrease upon stimulus, to better categorize the changes and identify signal from noise, we quantified pixel numbers of positive and negative signals as the following: the signal at pixel (x, y) is defined as positive, if

$$IOS_{t_i}(x,y)>\overline{IOS}(x,y)+3\sigma(x,y) \quad (2\text{-a})$$

Likewise, it is negative, if

$$IOS_{t_i}(x,y)<\overline{IOS}(x,y)-3\sigma(x,y) \quad (2\text{-b})$$

where

$$\overline{IOS}(x,y)=\frac{1}{n}\sum_{j=1}^{j=n}IOS_{t_j}(x,y) \quad (3)$$

$$\sigma(x,y)=\sqrt{\frac{1}{n}\sum_{j=1}^{j=n}\left(IOS_{t_j}(x,y)-\overline{IOS}(x,y)\right)^2} \quad (4)$$

where n is the pre-stimulus image number. For each dynamic differential IOS image, given the position of x_0, we counted the positive/negative pixel numbers along the y axis. In this way, we converted the 2-dimensional IOS image to a single line (one dimension). The value of each pixel in the line indicated the pixel numbers with positive /negative signals along the y axis (300 pixels). By combining such lines over time, we reconstructed the *x-t* spatiotemporal images (Fig. 3(a)).

There were spontaneous activities or granular patterns observed from IOS background images. Coefficient of variation (*CV*) [23] was used to quantify and represent the spontaneous activities:

$$CV(x,y)=\frac{\sigma(x,y)}{\overline{IOS}(x,y)} \quad (5)$$

Here, we call the array of *CV* as the texture image. For each trial, we had a texture image, and correspondingly, a quantitative approach was used to measure the uniformity and smoothness of the texture image [24]. The uniformity is defined as:

$$U=\sum_{k=0}^{k=L-1}H^2(CV) \quad (6)$$

where *H(CV)* is the histogram of the texture image, and *L* is the number of histogram bins. And the smoothness is defined as:

#159911 - $15.00 USD Received 12 Dec 2011; revised 19 Jan 2012; accepted 4 Feb 2012; published 20 Mar 2012

$$S = 1 - \left(\frac{1}{1 + \delta_{CV}^2} \right) \tag{7}$$

where δ_{CV}^2 denotes the variance over the whole texture image.

3. Results

3.1 Stimulus-evoked IOS comparison between WT and mutant mouse retinas

Figure 2 shows a dynamic differential IOS comparison between WT and *Cngb1* mouse retinas activated by a single flash. Each image (400 x 300 pixels) is an average over 200 images. Figure 2(a) shows a representative mouse retina image sequence. For each trial, pre-stimulus baseline recording was collected for 0.4 s (i.e., 200 frames) before a 10 ms visible white light stimulus was delivered. The black arrowhead (Fig. 2(a)) indicates the onset of stimulus. Figure 2(b) shows IOS images of 2- month-old WT mouse retina. Upon the stimulus, IOS image revealed a robust and rectangular pattern spread out over the stimulus activated region (Fig. 2 (b)). Under the same experimental conditions, IOS images of 2-month-old rod degenerated mouse retina also showed a regular rectangular pattern, however, due to ongoing retinal degeneration [21], signal strength was greatly attenuated (Fig. 2(c)). In 1-year-old mutant mice, visible light stimulus evoked optical signals were no longer detectable (Fig. 2(d)) due to the photoreceptor absence [21].

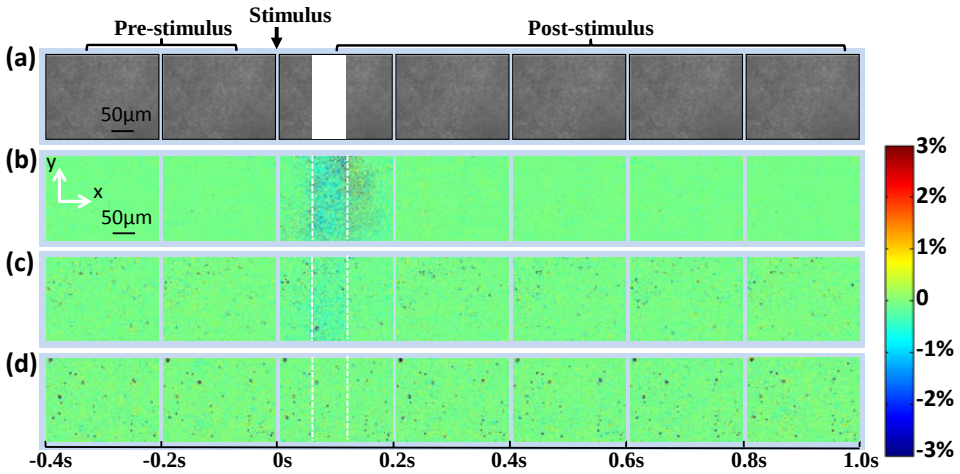

Fig. 2. (a) Representative images of a mouse retina. The white rectangle in the third frame showed the visible stimulus pattern. The black arrow indicated the delivery of stimulus light. (b) Dynamic differential IOS images of two-month-old WT mouse retina. (c) Dynamic differential IOS images of two-month-old mutant mouse retina. (d) Dynamic differential IOS images of 1-year-old mutant retina. Scale bars (in black) represent 50 μm.

In order to investigate spatial and temporal characteristics of the positive and negative IOSs, we depicted spatiotemporal images of the quantities of positive and negative signals in Fig. 3(a). The white dash lines in Fig. 3(a) indicated the stimulus edges. As shown in Fig. 3(a), positive and negative signals shared similar time courses and spread out around the stimulus area. Because of the comparable time courses of the overall positive and negative signals, to simplify analysis, we inverted the negative signals and used the absolute value of IOSs as the IOS magnitude to quantify the strength of the localized stimulus-evoked activities. In order to quantitatively investigate the response differences between WT and mutant retinas over time, the IOS magnitude curves corresponding to Fig. 2(b)-2(d) were plotted in Fig. 3(b). As shown in Fig. 3(b), the signal magnitude of 2-month-old WT retina

#159911 - $15.00 USD Received 12 Dec 2011; revised 19 Jan 2012; accepted 4 Feb 2012; published 20 Mar 2012

was more than five times larger than that in mutant retina of the same age. In 1-year-old mutant retina, IOS was not observed (Fig. 3(b)). Figures 3(c) and 3(d) show statistical analysis of IOS results based on 7 two-month-old WT and 11 two-month-old mutant mice. In addition to magnitude difference, the IOS of WT mouse retinas occurred and reached peak value earlier in comparison with that of mutant retinas (Fig. 3(d)), which was consistent with previous reported ERG changes [21, 25].

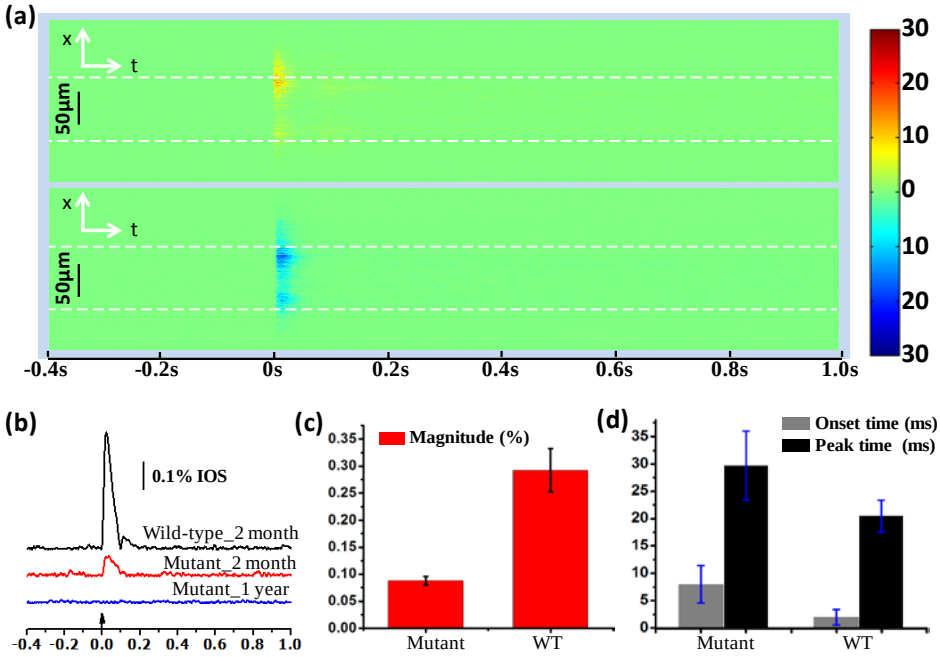

Fig. 3. (a) Spatiotemporal patterns of positive and negative IOS signals, corresponding to Fig. 2(b). The top panel is the image of positive pixel numbers and the bottom is negative signal pixel numbers. The unit of the color bar is pixel number. Scale bars (in black) represent 50 μm. The vertical axis (x) corresponds to the horizontal axis (x) in Fig. 2(b). The method to reconstruct spatiotemporal images was described in the section of data processing. (b) Dynamic IOS magnitude changes of the three retinas shown in Fig. 2(b)-2(d). (c) Statistical analysis of IOS magnitude of 7 two-month-old WT and 11 two-month-old mutant mouse retinas ($p<0.0001$). (d) Statistical analysis of corresponding IOS onset time ($p<0.0004$) and peak time ($p<0.002$).

3.2 Spontaneous activity in WT and mutant mouse retinas

Two-month-old *Cngb1* knockout mutant mice retinas did not show remarkable structural changes visually compared to WT mice (Fig. 4(a)). However, functional IOS images of the mutant retinas revealed irregular spatiotemporal patterns (Figs. 2(c)-2(d)). These irregular spontaneous changes occurred, without the requirement of retinal stimulation. Texture images (described in the data process section) of 4 trials of WT and mutant mouse retinas are shown in Fig. 4(b). In comparison with relative clean texture images of WT retinas, mutant retinas showed various sizes of granular like particles distributed randomly around the whole area. In order to better quantify their spatial differences, the smoothness and uniformity of texture images of 21 WT and 19 mutant mouse retinas were compared. Statistical analysis results showed texture image for WT was four times smoother (Fig. 4(c)) and significantly more homogeneous (Fig. 4(d)) as compared to the mutant.

#159911 - $15.00 USD Received 12 Dec 2011; revised 19 Jan 2012; accepted 4 Feb 2012; published 20 Mar 2012

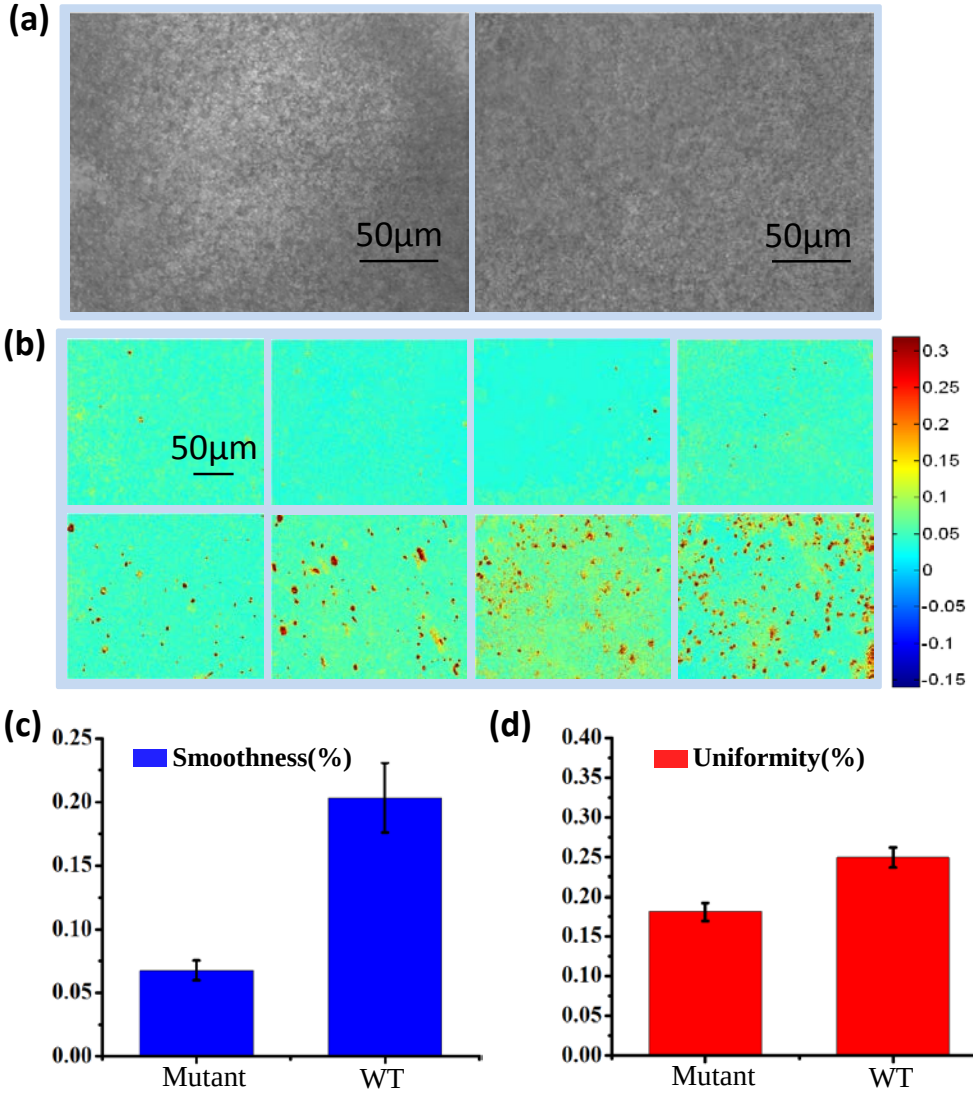

Fig. 4. (a) Raw structure images of 2-month-old WT (left) and mutant (right) mouse retinas; (b) Texture images of WT (top) and mutant (bottom) mouse retina. The texture images represent the strength of spontaneous activity over the pre-stimulus time. (c) Statistical analysis of background smoothness of 21 WT and 19 mutant mouse retinas ($p<0.0001$). (d) Statistical analysis of background uniformity ($p = 0.002$). Scale bars represent 50 μm.

4. Discussion

In summary, we compared stimulus-evoked IOS responses in normal and mutant retinas to demonstrate the feasibility of IOS identification of retinal dysfunction. Both 2-month and 1-year-old mice were measured. In 2-month-old mutant mice, time course and peak value of the stimulus-evoked IOS were significantly delayed (relative to stimulus onset) and reduced, respectively, compared to age-matched WT mice. In 1-year-old mutant mice, stimulus-evoked IOSs were totally absent.

Recent morphological study of Cngb1 gene knockout mice has revealed shorter and disorientated photoreceptor (rod) outer segments over the whole retina area [21], which might result in the reduced IOS response correlated with retinal stimulation. Moreover, functional defects of the photoreceptors might further affect the IOS response. Previous studies with

#159911 - $15.00 USD Received 12 Dec 2011; revised 19 Jan 2012; accepted 4 Feb 2012; published 20 Mar 2012

isolated photoreceptor outer segments and isolated retinas have demonstrated transient IOSs associated with phototransduction [26–28]. Both binding and release of G-proteins to photoexcited rhodopsin might contribute to the positive (increasing) and negative (decreasing) IOSs [27]. Localized biochemical processes might produce non-homogeneous light intensity changes, i.e. positive and negative signals mixed together. Besides the biochemical mechanism, physical changes, such as stimulus-evoked cell volume changes associated with water influx due to ionic currents through gated membrane channels might also contribute to the IOS response [29–32]. In Cngb1 gene knockout mice, it is established that the cyclic-nucleotide-gated cation channels regulating ion flow into rod photoreceptor outer segment are not functioning properly, which can reduce ion movement and light sensitivity of rod photoreceptor cells [21]. Therefore, stimulus-evoked IOS changes might be substantially reduced. For 1-year knockout mice, the photoreceptors, which are responsible for capturing photons and initiating phototransduction, were completely gone, and therefore no detectable stimulus-evoked IOS was observed (Figs. 2(d) and 3(b)).

In addition to overall changes of IOS magnitude (Fig. 3(c)) and time course (Fig. 3(d)), distinct spontaneous IOS patterns were observed in WT and mutant retinas. WT mouse retinas showed clean background baseline before retinal stimulation (Fig. 2(b), and first row of Fig. 4(c)). In contrast, mutant mice showed enhanced spontaneous IOS responses which might attribute to spontaneous activity at inner neural layers. It is known that mammalian retinal degeneration gradually proceeds from outer retina to inner neural network, from the death of rods and cones to dendrite truncation in bipolar cells or even entire neural network remodeling [25, 33]. Previous reports on rod degenerated mouse models have demonstrated that the loss of photoreceptors was accompanied by a marked increase of spontaneous activity in remnant neural networks [34]. Recent studies suggested that this spontaneous activity initiated at the presynaptic network including ON cone bipolar and AII amacrine cells [35]. At early stages, before major morphological modifications in the inner retina, of retinal degeneration, abnormal time course and magnitude of ERG b-wave has been observed [25].

We anticipate that fast IOS imaging may provide a supplemental method for better understanding of disease-associated retinal dysfunctions. In comparison with ERG recording, the IOS imaging can provide improved spatial resolution and three-dimensional imaging capability. Since Fast IOS imaging could be done noninvasively, it may lead to a new methodology for early detection of retinal dysfunction *in vivo*. High resolution IOS imaging will allow accurate disease detection and reliable treatment evaluation of age-related macular degeneration (AMD), retinitis pigmentosa (RP), diabetic retinopathy (DR), glaucoma, and other eye diseases that are known to produce retinal dysfunctions.

5. Conclusion

Unambiguous IOS abnormalities, in term of time course, magnitude, and spontaneous activity, were observed in *Cngb1* knockout mutant mouse retinas. Comparative study of WT and mutant mouse retinas demonstrates the potential of using IOS imaging for objective evaluation of disease-associated retinal dysfunctions. Further development of the IOS imaging technology may provide improved retinal disease study and diagnosis. Moreover, high spatiotemporal resolution IOS imaging may foster advanced understanding of disease-associated neural remodeling in the retina.

Acknowledgments

This research is supported in part by Dana Foundation (Brain and Immuno-Imaging Grant program); Eyesight Foundation of Alabama, NSF CBET-1055889, NIH R21 RR025788, NIH R21 EB012264, NIH R01 EY018143 and Vision Sciences Core grant NIH P30 EY03039.

#159911 - $15.00 USD Received 12 Dec 2011; revised 19 Jan 2012; accepted 4 Feb 2012; published 20 Mar 2012